DOI: 10.15255/KUI.2015.044
KUI-1/2016
Original scientific paper
Received September 30, 2015
Accepted November 18, 2015

Development Trend of the Compressive Strength of an In-Service Sidewall Corroded by Sulphate with a High Concentration of Ca^{2+}

W. He,[a] *X. Meng*,[b] *Y. Zheng*,[b] *H.-G. Ji*,[a*] and *C.-B. Liu*[c]

[a] School of Civil and Environmental Engineering,
University of Science and Technology Beijing, 100 083 Beijing, P.R. China
[b] Architectural Design and Research Institute of Tsinghua University co.,
LTD, 100 084 Beijing, P.R. China
[c] Beijing Vocational College of Agriculture, Department of Hydraulic and
Architectural Engineering, 102 442 Beijing, P.R. China

Abstract

At the bedrock section of the auxiliary shaft of the Tong-ting coal mine, the sidewall has varying degradation degrees in different parts. The part on which water flowed is barely corroded, whereas the moist part near the pouring joints is seriously corroded. We first studied the mechanism of this phenomenon by chromatography, X-ray diffraction, and energy-dispersive X-ray spectroscopy. We then used simplified models built by particle flow code software (*i.e.*, particle flow code in three dimensions, PFC3D) to analyse how increasing degradation depth affects compressive strength and failure patterns. The results were as follows. (1) Gypsum and calcite in corrosive water were supersaturated. The part on which water flowed was protected by the crystallized precipitation on the concrete. By contrast, the degradation of the part where water flowed through pouring joints was aggravated by internal crystallization and dissolution. (2) PFC3D numerical simulation indicated that decreases in vertical ultimate stress were strongly linearly correlated with degradation depth. As for the −355.5 m damaged part, reinforcement should be conducted before degradation depth reaches 250 mm. (3) No obvious signs were observed prior to the failure of the corroded sidewall. Therefore, the development of degradation depth should be monitored before degradation parts are reinforced.

Keywords

Site investigation, groundwater, degradation, failures, stress analysis

1. Introduction

An auxiliary shaft is the only entrance for transporting staff and equipment; as such, its service life typically lasts more than 50 years, and its safety is of the utmost importance to a coal mine.[1] The sidewall of vertical shafts is often exposed to a complex stress environment, and formations nearby contain substantial amounts of aggressive ions, such as SO_4^{2-}, Mg^{2+}, and Cl^-. Many scholars[2,3] posit that SO_4^{2-} and Cl^- are the main factors causing underground structure degradation. However, limited research has been conducted on the influence of several "non-aggressive" ions, such as Ca^{2+}.

Caused by exposure of concrete to sulphate ions and moisture, sulphate attack is due to a series of chemical reactions between sulphate ions and principle components of the cement paste microstructure. Sulphate attack processes decrease the durability of concrete by changing the chemical nature of the cement paste, and the mechanical properties of the concrete. This chemical process occurs when the sulphate ions react with ionic species of the pore solution and hydrated products of cement to form ettringite, gypsum or thaumasite or mixtures of these phases.[4] The precipitation of these solid phases can lead to strain within the cement-based materials, inducing expansion, strength loss, spalling, and severe degradation.[5]

The groundwater of the Huang-Huai region contains high concentrations of SO_4^{2-} and Ca^{2+}, and several vertical shafts at the bedrock section have been seriously corroded. In general, groundwater penetrates into the vertical shafts through two pathways: (1) by flowing out of the construction holes drilled during cageway girder installation; and (2) by flowing through pouring joints. When corrosive water flows on the inner wall, a dense layer forms on the saturated surface. The part under the dense layer is barely corroded, whereas the part where water flows through the pouring joint is seriously corroded. Considering the auxiliary shaft of the Tong-ting coal mine as the research object, we studied the mechanism of different degradation degrees of different parts. Although structural safety declines after degradation, reinforcement is unnecessary if the bearing capacity of the corroded shaft meets the safety design requirements. The deepest degradation was found in the −355.5 m damaged part; as such, this part was considered in building simplified models by particle flow code in three dimensions (PFC3D) to analyse the compressive strength and failure pattern as degradation depth increased.

---

[*] Corresponding author: Professor Hongguang Ji
e-mail: jihongguang@ces.ustb.edu.cn

2. Experimental: Degradation mechanism analysis

During the construction period, the subsection pouring method was adopted at the bedrock section of the auxiliary shaft of the Tong-ting Coal Mine. The general process of the subsection pouring method can be described as follows: drilling holes into rocks and filling them with explosives, detonating the explosives, ventilating and removing the slag, constructing the framework, pouring concrete. Given the unavoidable placing intermission, the glue between pouring blocks was weak, and a hydraulic pathway had formed.

Many construction holes were also drilled into the sidewall during cageway girder installation. The inner wall near the pouring joint at the bedrock section is moist but has no obvious flowing water. The flow rate from construction holes is typically more than 1 l min^{-1}.

2.1 Ion composition analysis of corrosive water

Three major damaged parts occurred in the auxiliary shaft of the Tong-ting Coal Mine, and they were located at −346, −355.5, and −357 m. The three parts were near pouring joints. Water was difficult to collect because the flow rate through the pouring joints was low. Thus, water from −391 and −419 m construction holes was extracted for analysis. In accordance with the "Code for investigation of geotechnical engineering",[6] the water samples were analysed by using an ICS-5000 ion chromatographer. The results are shown in Table 1.

Table 1 indicates that the two samples have nearly the same chemical composition and concentration. The major ions from highest to lowest content are SO_4^{2-}, Na^+, Ca^{2+}, and Mg^{2+}. The average concentration of SO_4^{2-} is greater than 1000 mg l^{-1}; such a concentration is classified as "serious degradation degree" according to the "Code for durability design of concrete structures".[7] The average ion products of gypsum ($CaSO_4$) and calcite ($CaCO_3$) in the water samples are $1.17 \cdot 10^{-4}$ and $8.38 \cdot 10^{-3}$, respectively. These values are higher than the solubility product constant K_{sp} of gypsum and calcite ($7.1 \cdot 10^{-5}$ and $4.96 \cdot 10^{-9}$ at 25 °C). Hence, gypsum and calcite in the water samples are supersaturated, and crystallized in the inner concrete wall near the pouring joint.

The chemical compositions of the water samples are quite different from a representative concrete pore solution, which led to the effect of medium transfer between the groundwater and the sidewall. Percolating groundwater along pathways through concrete efficiently leaches alkalis and portlandite, leading to a "leaching zone" characterized by the reduction of portlandite, $Ca(OH)_2$. During further leaching, the density of the hardened cement paste is reduced accompanied by microcracking and therefore the permeability properties increase. Therefore, with the co-action of internal crystallization and dissolution, the sulphate attack in this part is aggravated.

2.2 Component analysis of the corroded concrete and the dense layer

In the damaged parts, the concrete near the pouring joint is subject to severe bulging and cracking. The paste matrix is characterized by graininess, and the bond between the paste matrix and the aggregate is weak. The most seriously damaged part is located at −355.5 m. The bulging layer at −355.5 m is approximately 80 – 100 mm in depth and 200 mm in height. The photographs in Fig. 1.1 and 1.2 were captured before and after the degradation layer of the −355.5 m damaged part was shovelled; the tape in Fig. 1.2 was placed to demonstrate the contrast. As shown in Fig. 1.1, the surface of the bulging part, which is slightly covered by white powder, is rough and higher than the nearby surfaces. The corrosive water from construction holes flows on the inner wall and is collected at the reservoir at the shaft bottom. As shown in Figs. 2.1 and 2.2 (which were captured at −430 and −390 m, respectively), the sidewall surface is flat and non-corroded under the protection of the dense layer.

Fig. 1 – Corroded concrete at −355.5 m
Slika 1 – Korodirani beton na −355,5 m

Table 1 – Ion content of the water samples
Tablica 1 – Ionski sastav uzoraka vode

Serial number Serijski broj	γ/mg l^{-1}								pH
	Na^+	Ca^{2+}	Mg^{2+}	F^-	Cl^-	NO_3^-	CO_3^{2-}	SO_4^{2-}	
1	655.5	256.9	84.07	0.23	184.27	1.43	83.31	1873.9	7.72
2	708.3	215.0	69.02	0.25	168.64	<0.05	86.58	1928.2	7.65
average prosjek	681.9	236.0	76.54	0.24	176.46	–	84.94	1901.0	7.69

Fig. 2 – Non-corroded sidewall with a cleared dense layer
Slika 2 – Nekorodirani bočni zid sa skinutim kompaktnim slojem

Using a Rigaku Ultima-IV X-ray diffractometer with Cu radiation operated at 40 kV and 40 mA in air, we collected a corroded concrete sample from the −355.5 m damaged part and a dense layer sample from −430 m for testing. The results of the X-ray diffraction (XRD) analysis are shown in Figs. 3 and 4.

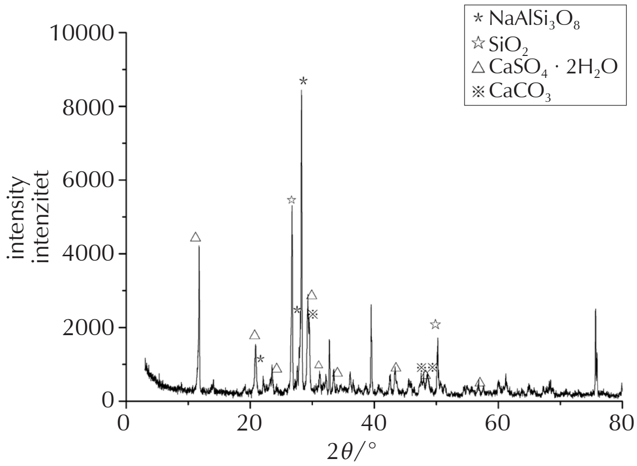

Fig. 3 – XRD analysis of the corroded concrete
Slika 3 – Rendgenska difrakcijska analiza korodiranog betona

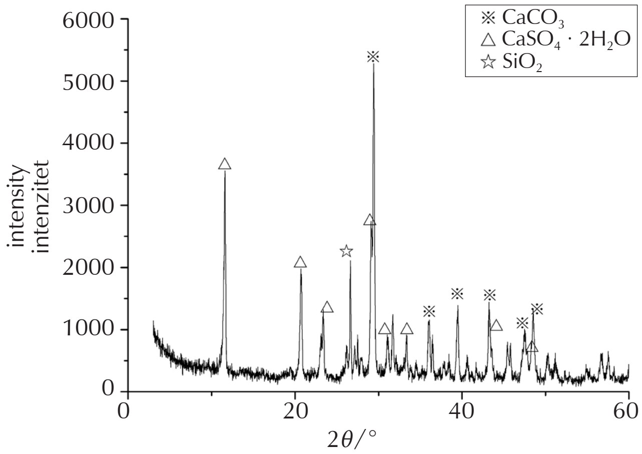

Fig. 4 – XRD analysis of the dense layer
Slika 4 – Rendgenska difrakcijska analiza kompaktnog sloja

Fig. 3 shows that the corroded concrete mainly consists of albite ($NaAlSi_3O_8$), quartz (SiO_2), gypsum ($CaSO_4 \cdot 2\,H_2O$), and calcite ($CaCO_3$). Portlandite, which is one of the main constituents of common concrete, was not found in the corroded concrete sample. On the contrary, gypsum, which is hardly found in common concrete, is the main stage.

According to different phenomena and degradation products, sulphate degradation can generally be divided into five types, namely, sulphate, ettringite, gypsum, thaumasite, and magnesium sulphate crystalline degradation. Degradation type is highly correlated with the temperature, pH value, and sulphate concentration of the corrosive water. For example, sulphate crystalline degradation typically occurs when the pH is less than 10.5, the concentration of SO_4^{2-} is greater than 1000 mg l^{-1}, and the major degradation product is gypsum. The average pH value and concentration of SO_4^{2-} in the water samples are 7.69 and 1901.05 mg l^{-1}, respectively. The main stage of the corroded concrete is gypsum. Therefore, the degradation type may be sulphate crystalline degradation. The reaction formula of this degradation type is as follows:

$$\begin{aligned} &Ca(OH)_2 \ + \ SO_4^{2-} \ + \ 2\,H_2O \ \rightarrow \\ &\rightarrow \ CaSO_4 \cdot 2\,H_2O \ + \ 2\,OH \end{aligned} \qquad (1)$$

As shown in Fig. 4, the main components of the dense layer are calcite ($CaCO_3$), gypsum ($CaSO_4 \cdot 2\,H_2O$), and quartz (SiO_2), which are the same as the components of the corrosive water. A FEI Quanta 250 FEG scanning electron microscope was used to observe the microstructure of the dense layer, and the observations are shown in Fig. 5. The magnification of Fig. 5 is 5000.

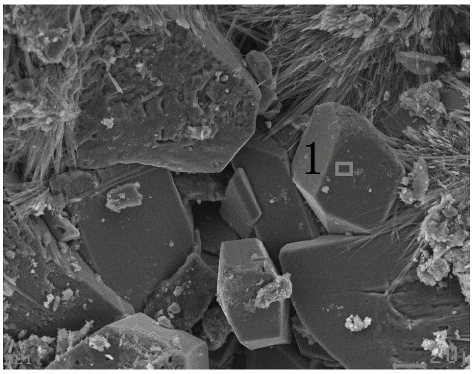

Fig. 5 – SEM image of the dense layer
Slika 5 – SEM slika gustog sloja

Table 2 – EDS elemental analysis result
Tablica 2 – Rezultati elementne analize EDS-om

Element	C	O	S	Ca
w/%	10.48	28.84	21.78	38.44

The results of scanning electron microscopy and EDS show that the gypsum in the dense layer is predominantly at glassy state. As shown in Fig. 5, owing to the compact structure of the glassy gypsum, the water permeability of the dense layer is low, thereby protecting the shaft concrete against the corrosive effect of the corrosive water.

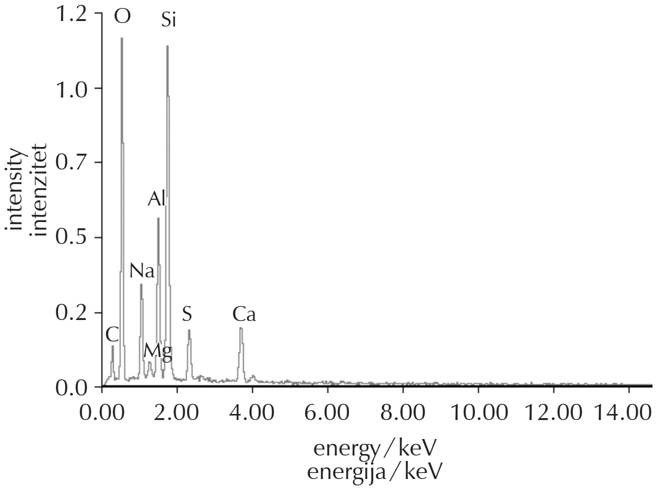

Fig. 6 – Energy-dispersive X-ray spectrum of the dense layer
Slika 6 – Energijski disperzivni rendgenski spektar kompaktnog sloja

Although the cracks of the pouring joint grows because of the coupling effects of the formation pressure, the gravity exerted on the sidewall, and the degradation attack of the corrosive water, the flow rate through the pouring joint is reduced because the cracks become compact under high stress. Concrete water easily volatilizes because of the high-speed air flow in the auxiliary shaft, which is one of the intake airways in a coal mine. Therefore, the gypsum and calcite in corrosive water are crystallized in the inner concrete wall near the pouring joint, and the sulphate attack is aggravated at this part.

In summary, crystal stress is the major cause of concrete degradation near pouring joints. This conclusion is coincident with the findings of other studies.[8,9,10]

Given that the gypsum and calcite in corrosive water are supersaturated, a dense layer is formed by the crystallized precipitation of gypsum and calcite when water flows on the inner wall. Therefore, not only the inner wall of the shaft, but the outer wall as well, is protected by the supersaturated corrosive water from sulphate attacks.

3. Results and discussion: PFC3D simulations of sidewall

Degradation damage is harmful to the structural reliability of auxiliary shafts, which are the only entrance points for transporting staff and equipment. The auxiliary shaft of the Tong-Ting coal mine has three major damaged parts, which are not far from one another. As such, the formation properties of these parts are similar. The −355.5 m damaged part, which contains the deepest degradation depth, was considered the research object. PFC3D models with different degradation depths were built to analyse the degeneration of compressive strength and failure patterns.

3.1 Establishment of PFC3D models

The rocks at the bedrock section are homogeneous (mainly sandstone or mudstone). The stratum inclination is low (approximately 5° – 15°), and the degradation depth is almost axisymmetric. Thus, by symmetric constraint, we utilized $\frac{1}{8}$ of the sidewall to establish a numerical model. The height of the simplified model was assumed to be 2.0 m to reduce the stress concentration effect.

Given that the bedrock section sidewall is under a uniform load, any vertical section shear is zero. The fraction and normal displacement of the two vertical planes were set to zero. The upper and lower planes are two load planes that load or unload the sample by moving along the vertical axis. The side face of the model is a servo plane that keeps the confining pressure constant through expansion or contraction. The fractions of the upper and lower planes were set to the same values as the contacts. Using the Fish language built in PDC3D, we programmed a loading procedure based on the numerical servo-mechanism.[11] During the loading procedure, the vertical strain rate was 0.025 s^{-1} to maintain the model at static equilibrium. The boundary conditions for the numerical simulation are shown in Fig. 7.

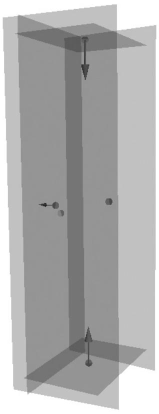

Fig. 7 – Boundary conditions
Slika 7 – Granični uvjeti

Contact-bonded and parallel-bonded models are two widely used bond behaviours. The parallel-bonded model is more appropriate for concrete than the contact-bonded model because the former can transmit both forces and moments at the contact point among particles. For this reason, the parallel-bonded model was used in this study.

No mathematical relationship exists between microscopic and macroscopic parameters. Therefore, numerical simulation experiments were conducted to obtain microscopic parameters. In this simulation, the minimum radius of the balls was 12 cm, the ratio of the maximum radius to the minimum radius was 1.66, and the particle diameter distribution obeyed Gauss distribution. The concrete grade of the sidewall at the bedrock section was C30. The uniax-

Table 3 – Microscopic parameters
Tablica 3 – Mikroskopski parametri

$\rho/\text{kg m}^{-3}$	μ	ba_Ec/MPa	pb_Ec/MPa	pb_kn/MPa		pb_ks/MPa	
				mean srednja vrijednost	deviation odstupanje	mean srednja vrijednost	deviation odstupanje
2600	0.4	$4.00 \cdot 10^3$	$2.00 \cdot 10^3$	21	2.1	31	3.1

ial compressive strength and elastic modulus of C30 were 30 MPa and $30 \cdot 10^4$ N mm^{-2}, respectively. When the microscopic parameters (Table 3) were assigned, the uniaxial compressive strength and elastic modulus of the PFC3D model were 32 MPa and $28 \cdot 10^4$ N mm^{-2}, respectively. Thus, the microscopic parameters in Table 3 were adopted in the simulation. In Table 3, friction is the particle friction coefficient, ba_Ec is the Young's modulus at each particle-particle contact, pb_Ec is the Young's modulus of each parallel bond, pb_kn parallel-bond normal stiffness, pb_ks is the parallel-bond shear stiffness.

The pouring joint was simulated as a joint plane created with the JSET command. The position was specified by the DIP and ORIGIN keywords, and the weak properties were assigned on the plane. Given that the structure of the corroded concrete is loose and the bearing capacity is low, the particles in the corroded part were deleted in the simulation. A population of particles with an artificially small radius was created within the specified volume to improve the generation speed. Small-radius particles were easy to place in this manner because the available void space was large. The particles were then expanded until the desired porosity was obtained. The total numbers of particles of the 0, 100, 175, and 250 mm degradation-depth models were 21372, 21157, 20977, and 20791, respectively, as shown in Fig. 8.

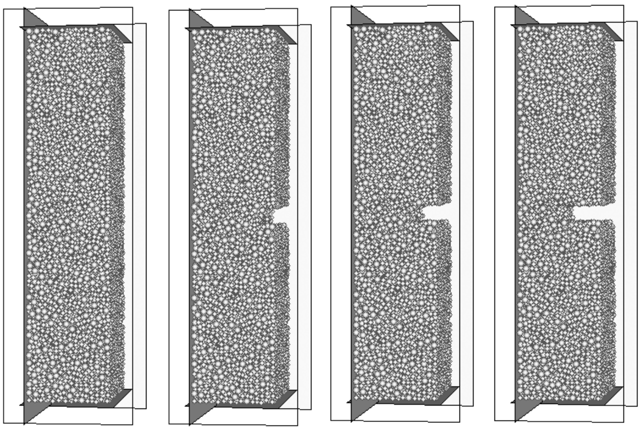

Fig. 8 – Simplified shaft models with different degradation depths
Slika 8 – Pojednostavljeni modeli okna s različitim dubinama degradacije

3.2 External forces on the simplified models

External forces on the sidewall can be divided into two types, namely, (1) lateral pressure p_h, which includes formation and water pressure; and (2) vertical pressure p_v, which includes the gravity of the sidewall and the equipment, as well as negative friction force.[12] Although no groundwater is present and the cohesion of the surrounding rock is low, the lateral pressure on the outer wall can be calculated with the following formula:[13]

$$p_\text{n}^\text{u} = \left(\sum_{i=1}^{n-1} \rho_i \, h_i \right) K_\text{n} \tag{2}$$

where K_n is the lateral pressure coefficient of i-th formation; ρ_i and h_i are the bulk density and thickness of i-th formation, respectively. The average bulk density and the lateral pressure coefficient were assumed to be 2300 kg m^{-3} and 0.164, respectively. The lateral pressure on the sidewall at −355.5 m was 1.32 MPa.

The ultimate stress of the sidewall includes vertical and radial ultimate stresses. The vertical ultimate stress refers to the maximum vertical load while the lateral pressure remains invariant. The radial ultimate stress is almost the same. At the bedrock section of the Tong-ting shaft, the formation and the lateral pressure are stable. Thus, our study focused on the vertical ultimate stress as degradation depth increases.

3.3 Crack count (CC)

Crack initiation stress and crack damage stress are two important indicators in the failure process of the shaft sidewall. The crack initiation stress marks crack initiation and stable propagation. When the stress exceeds the crack damage stress, crack growth becomes unstable, and rock dilation begins. In the parallel-bonded model, bond breakage causes the bonding stiffness to become inactive, resulting in stiffness reduction. In this respect, the CC recorded in every n steps can be used to characterize the damage degree.[14]

In the PFC3D simulations, if the cracks in each step were regarded as an event, then the obtained result would be large in randomness and weak in representativeness. By making comparisons, we treated the CC in every 20 steps as one event.

3.4 Analyses of the numerical calculation results

3.4.1 Relationship between vertical ultimate stress and degradation depth

A recent study[15,16] demonstrated that the failure law greatly influences stress states. As the loads become more complex, the shaft sidewall becomes subjected to a three-directional pressure. The sidewall concrete is reinforced by the confining pressure. The formula for calculating the vertical ultimate stress is as follows:

$$p_{\mathrm{v}}^{\mathrm{b}} = 5.935\left(d/r\right)^{0.2922}\sigma_{\mathrm{c}}^{0.7461}\,p_{\mathrm{h}}^{0.1417} \quad \left(p_{\mathrm{h}} > 0.5\,\mathrm{MPa}\right) \tag{3}$$

where d and r are the thickness and inside radius of the sidewall, respectively, and p_{h} is the lateral pressure on the sidewall.

As for the sidewall of the Tong-ting shaft at the bedrock section, d, r, σ_{c}, and p_{h} were 0.45 m, 3.4 m, 21 MPa, and 1.32 MPa, respectively. The calculated vertical ultimate stress $p_{\mathrm{v}}^{\mathrm{b}}$ was 31.73 MPa, which was close to the PFC3D result of 34.1 MPa. These values suggest that the simplified PFC3D models can achieve satisfactory calculation accuracy. Fig. 9 shows the relationship between degradation depth and vertical ultimate stress based on PFC3D simulations.

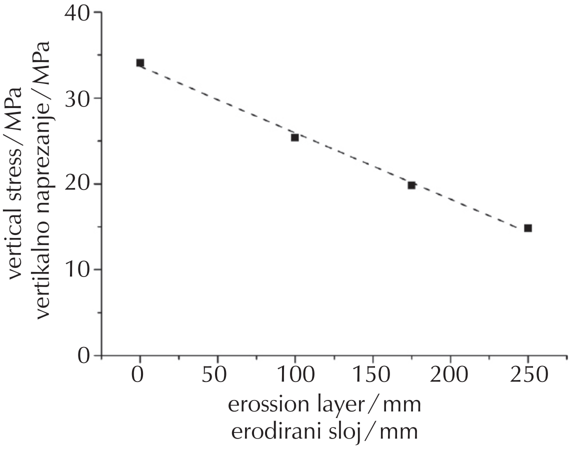

Fig. 9 – Relationship between vertical ultimate stress and degradation depth

Slika 9 – Odnos između maksimalnog vertikalnog naprezanja i dubine degradacije

The result showed a good linear relation between vertical ultimate stress and degradation depth in the range of 0–250 mm. The linear equation was $p_{\mathrm{v,t}}^{\mathrm{b}} = -0.0773h_{\mathrm{t}} + 33.673$, and the related coefficient was 0.998. When the degradation depth reached 250 mm, the vertical ultimate stress was 14.8 MPa, which was less than the design value of 14.87 MPa. Reinforcement should be conducted before the degradation depth reaches 250 mm.

3.4.2 Stress–strain and CC curves

Stress–strain and CC curves with different degradation depths are shown in Fig. 10. The monitoring points C, D, and F in Fig. 10 represent the proportional limit, ultimate stress, and CC peak point, respectively. The portion of the curve between the origin and point A was a straight line. In this portion, no initial stress or strain occurred. Up to point C, Hooke's law was obeyed according to which stress was directly proportional to strain. Point C was thus known as the proportional limit. Point D indicated the location of the value of the ultimate stress. The PFC3D model was considered to have completely failed once it reached the ultimate stress.

Fig. 10(a) shows that owing to the confining pressure, the vertical ultimate stress of the non-corroded model was 34.1 MPa, which was higher than that of C30 concrete (16.7 %). The stress was obviously reduced with a turning point at the stress peak, and the fracture mode was brittle fracture. In Figs. 10(b)–(d), the increasing degradation depth not only decreased the vertical strength but also the strain at the peak point. When the degradation depths were 0, 100, 175, and 250 mm, the vertical strains at the peak point were $3.05 \cdot 10^{-3}$, $2.72 \cdot 10^{-3}$, $2.44 \cdot 10^{-3}$, and $2.21 \cdot 10^{-3}$, respectively. When the degradation depths were 0, 100, 175, and 250 mm, the ratios between the strain at the proportional limit stress and peak stress were 0.918, 0.912, 0.857, and 0.751, respectively. The elastic portion of the stress–strain curve decreased rapidly.

In Fig. 10, the process of model failure can be divided into four stages, viz., the beginning stage (I), the rising stage (II), the tempestuousness stage (III), and the drop stage (IV). At the preliminary stage of loading, *i.e.*, the beginning stage (I), stress increased as a linear elastic feature. At the compression stage (Segment OA), no cracks were generated. The first crack occurred at point A, and the initiation crack stresses were 19.36, 13.92, 12.99, and 9.07 MPa. At the rising stage (II), CC showed a steady increasing tendency.

In Figs. 10 (a)–(b), only one CC peak occurred right after the stress peak was reached. When the strain–stress curve entered the failure stage, the model destructed rapidly. The position of the major CC peak in Figs. 10(c)–(d) was almost the same as the position in Figs. 10(a)–(b). In Figs. 10(a)–(b), aside from the major CC peak, a small CC peak occurred between the beginning stage (I) and the rising stage (II). The fracture failure process is also a process of releasing energy. In Figs. 10(c)–(d), the plastic portion of the stress–strain curve increased because some energy was released at the second CC peak before breaking.

Fig. 11 is a side view of the crack shapes of different degradation depths at the proportional limit stress. The black and grey points in Fig. 11 represent the shear and tensile cracks, respectively. In Fig. 11, nearly all cracks were shear cracks. Cracks were in homogeneous distribution in the non-corroded model. With an increase in degradation depth, the distribution of cracks gradually gathered at the bottom because of the stress concentration at the bottom of the damaged part. At the proportional limit point, the sidewall models with degradation depths of 0, 100, 175, and 250 mm contained a total of 1187, 644, 269, and 68 cracks, respectively.

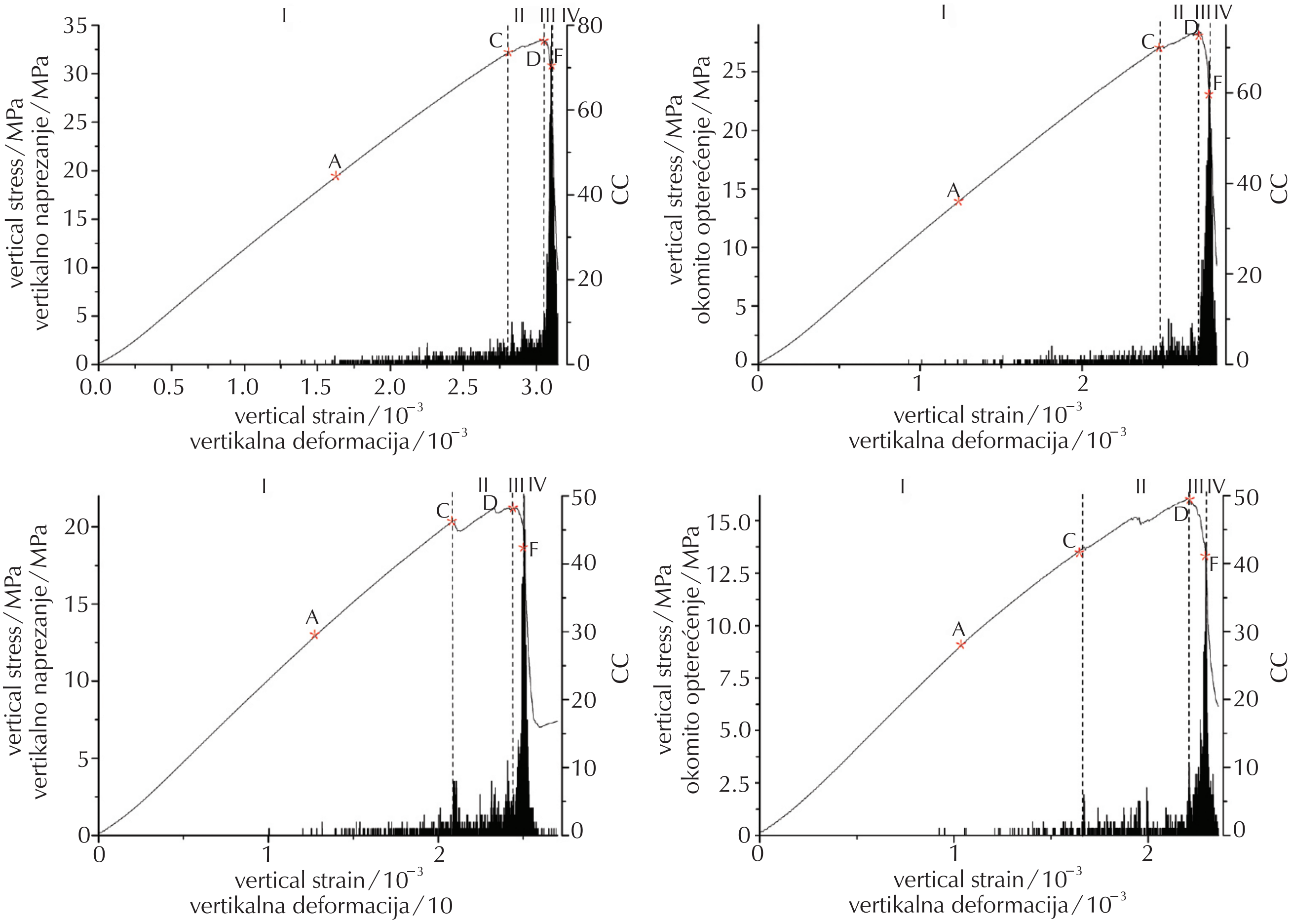

Fig. 10 – Stress–strain and CC curves with different degradation depths
Slika 10 – Dijagram naprezanja i CC s različitim dubinama razgradnje

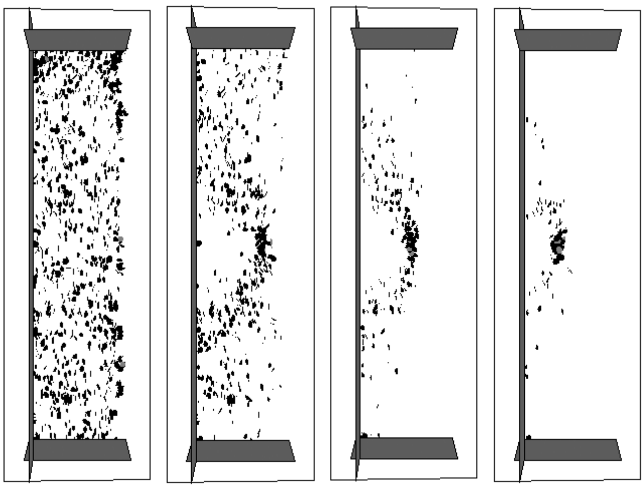

Fig. 11 – Crack shapes with different degradation depths at the proportional limit
Slika 11 – Oblici pukotina pri različitim dubinama propadanja na granici proporcionalnosti

At the ultimate stress point D, CC increased rapidly. The PFC3D models were at the tempestuousness stage (III). At this stage, CC increased rapidly, and the structure of the shaft models transformed into unstable state. Fig. 12 is a side view of the crack shapes of different degradation depths at point D.

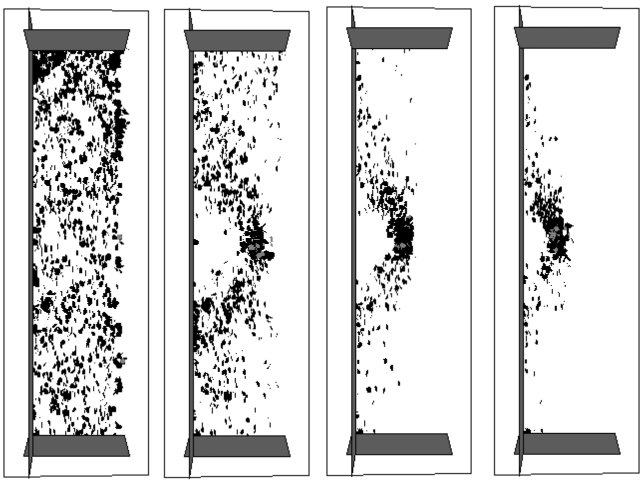

Fig. 12 – Crack shapes with different degradation depths at ultimate stress
Slika 12 – Oblici pukotina pri različitim dubinama propadanja pri tlačnoj čvrstoći

When a bond broke either for tensile or shear failure, a new microcrack formed in PFC3D. Fig. 12 shows the distribution of microcracks at ultimate stress. As shown in Fig. 12(a), the microcracks in the non-corroded model were almost uniformly dispersed, and the bearing capacity of the concrete was fully used. With an increase in the degradation depth near the pouring joint, the distance between the central axis of vertical loads and the section centroid where the concrete degradation increased, the distribution of microcracks concentrated on the upper and lower shear planes. Even when the degradation depth was 100 mm, no obvious sign occurred on the inner wall before failure, which was dangerous. Given that the sidewall models with degradation depths of 0, 100, 175, and 250 mm contained a total of 2477, 1470, 1193, and 633 cracks at the ultimate stress point, respectively, the energy release at the ultimate stress point decreased with an increase in degradation depth.

In Fig. 13, the relative strain was the ratio between the current strain and the strain at the peak stress. Although the degradation depth differed, the CC of all four simplified models began to rise at the same relative strain of 0.55. With an increase in degradation depth, the CC–relative strain curve was rough, and the amplitude of the portion of the curve increased before the ultimate stress had reduced.

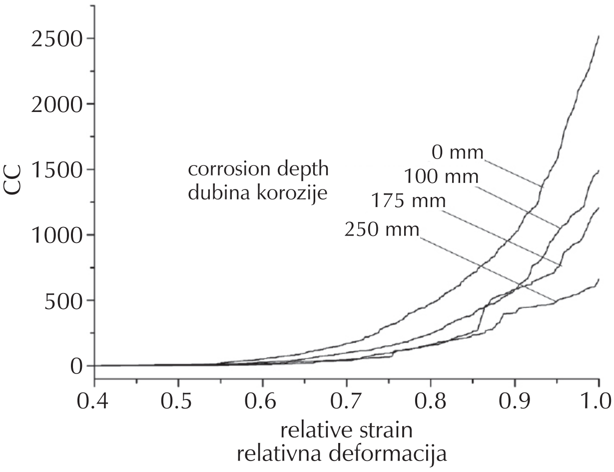

Fig. 13 – CC–relative strain curve with different degradation depths

Slika 13 – Odnos broja pukotina i relativne deformacije uz različite dubine razgradnje

4. Conclusions

Although Ca^{2+} in a sulphate solution is supersaturated and concrete is compact, the crystallized precipitation forms a dense layer on the concrete. The concrete is protected by this dense layer against sulphate attacks. When transverse cracks exist in the concrete, gypsum is crystallized in the inner concrete wall, and the sulphate attack is aggravated. Therefore, the effect of certain "non-aggressive" ions should be considered in sulphate attacks.

Owing to the strengthening effect of the confining pressure, the vertical ultimate stress of the sidewall is higher than the uniaxial compressive strength of concrete (16.7 %). At the −355.5 m damaged part, the decreases in vertical ultimate stress show a strong linear correlation with degradation depth. When the degradation depth at −355.5 m reaches 250 mm, the bearing capacity of the sidewall is insufficient, and reinforcement should be performed before that point.

As for the non-corroded sidewall, obvious cracks appear in the inner wall before failure, and the CC of the non-corroded sidewall model at ultimate stress is 2477. With increasing degradation depth, no obvious sign occurs before failure, and the CC at ultimate stress decreases obviously. When the degradation depth is 250 mm, CC is only 633.

ACKNOWLEDGEMENTS

The research work presented in this paper is sponsored by the National Basic Research Program of China ("973" Program) (Grant nos. 2010CB226803 and 2010CB731501) and the National Natural Science Foundation of China (Grant no. 51174015). The authors are grateful for their support.

List of abbreviations and symbols
Popis kratica i simbola

PFC3D	– particle flow code in three dimensions – kôd toka čestica u tri dimenzije
XRD	– X-ray diffraction – rendgenska difrakcija
EDS	– energy-dispersive X-ray spectroscopy – energijski disperzivna rendgenska spektroskopija
SEM	– scanning electron microscope – pretražni elektronski mikroskop
CC	– crack count – broj pukotina
γ	– mass concentration, $\mathrm{mg\,l^{-1}}$ – masena koncentracija, $\mathrm{mg\,l^{-1}}$
K_{sp}	– solubility product constant – konstanta produkta topljivosti
w	– mass fraction, % – maseni udjel, %
ρ	– density, $\mathrm{kg\,m^{-3}}$ – gustoća, $\mathrm{kg\,m^{-3}}$
μ	– friction factor – faktor trenja
ba_Ec	– Young's modulus at each particle-particle contact, MPa – Youngov modul na kontaktu čestica, MPa
pb_Ec	– Young's modulus of each parallel bond, MPa – Youngov modul na kontaktu čestica, MPa
pb_kn	– parallel-bond normal stiffness, MPa – normalna krutost paralelne veze, MPa
pb_ks	– parallel-bond shear stiffness, MPa – posmična krutost paralelne veze, MPa
p_h	– lateral pressure on the outer wall of the sidewall, MPa – bočni tlak na vanjskoj strani bočnog zida, MPa

p_n^u – calculated lateral pressure on the outside of the sidewall, MPa
– izračunati bočni tlak na vanjskoj strani bočnog zida, MPa

K_n – lateral pressure coefficient of the *i*-th formation
– koeficijent bočnog tlaka *i*-tog sloja

ρ_i – bulk density of the *i*-th formation, kg m^{-3}
– gustoća *i*-tog sloja, kg m^{-3}

h_i – thickness of the *i*-th formation, m
– debljina *i*-tog sloja, m

p_v^b – calculated vertical ultimate bearing capacity, MPa
– izračunata maksimalna vertikalna nosivost, MPa

d – thickness of the sidewall, m
– debljina bočnog zida, m

r – inside radius of the sidewall, m
– unutarnji promjer bočnog zida, m

σ_c – axial compressive strength of concrete, MPa
– osna tlačna čvrstoća betona, MPa

$p_{v,t}^b$ – vertical ultimate compressive capacity, MPa
– maksimalna vertikalna tlačna čvrstoća, MPa

h_t – degradation depth, mm
– dubina propadanja, mm

References
Literatura

1. *G. X. Cui, W. H. Yang, H. L. Lv*, Frozen Wall and sidewall in thick overburden, China University of Mining and Technology Press, 1998, Beijing, PR China, pp. 52–54.
2. *C. X. Wang*, The durability of shield tunnel, Undergr. Eng. Tunn. **2** (2002) 2–5.
3. *X. X. Ji, X. G. Wang, K. Wang, M. T. Cai,* Analysis and research on durability of concrete used in underground engineering structure, J. Wuhan University of Technology **28** (8) (2006) 43–45.
4. *C. Norah*, The occurrence of thaumasite in modern construction −A review, Cement Concrete Comp. **24** (4) (2002) 393−402.
5. *K. L. Ma, G. C. Long, Y. J. Xie*, Railway tunnel concrete lining damaged by formation of gypsum, thaumasite and sulphate crystallization products in southwest of China, J. Central South University of Technology **19** (2012) 2340–2347, doi: http://dx.doi.org/10.1007/s11771-012-1280-2.
6. MOHURD (Ministry of Housing and Urban-Rural Construction of the People's Republic of China) (2009) GB 50021-2009: Code for investigation of geotechnical engineering. Chinese Building Industry Press, Beijing, China.
7. MOHURD (Ministry of Housing and Urban-Rural Construction of the People's Republic of China) (2008) GB 50476-2008: Code for durability design of concrete structures. Chinese Building Industry Press, Beijing, China.
8. *N. Tsut, R. J. Flattr, G. W. Scherer*, Crystallization damage by sodium sulphate. J Cult. Herit. **4** (2) (2003) 109–115, doi: http://dx.doi.org/10.1016/S1296-2074(03)00022-0.
9. *R. J. Flattr, G. W. Schutter*, Hydration and crystallization pressure of sodium sulphate: a critical review, Mater. Res. Soc. Symp. Proc. **712** (2002) 29–34.
10. *C. Rodriguez-Navarro, E. Sebastian, E. Doehne*, How does sodium sulphate crystallize implications for the decay and testing of building materials, Cem. Concr. Res. **30** (10) (2000) 1527–1534, doi: http://dx.doi.org/10.1016/S0008-8846(00)00381-1.
11. ITASCA Consulting Group, Inc. (2008) PFC 3D theory and background. Itasca Consulting Group, Minnesota, USA.
12. *J. J. Yang*, Failure and strength characteristics of concrete sidewall, J. China Coal Society **23** (3) (1998) 246–251.
13. *J. P. Li*, Rock mechanics in mine. Metallurgical Industry Press, 2011, Beijing, PR China.
14. *K. Mu, T. B. Li, J. Yu*, Mesoscopic simulation of relationship of acoustic emission and compressive deformation behaviour in sandstone under confining pressures effect, Chinese J. Rock Mech. Eng. **33** (S1) (2014) 2786–2792.
15. *Z. H. Cheng, Y. F. Fu, C. A. Tang*, An Confining pressure effect on acoustic emission during rock failure, Chinese J. Rock Mech. Eng. **16** (1) (1997) 65–70.
16. *T. N. Gowd, F. Rummel*, Effect of confining pressure on the fracture behaviour of a porous rock, Int. J. Rock Mech. Min. **17** (12) (1980) 225–229, doi: http://dx.doi.org/10.1016/0148-9062(80)91089-X.

SAŽETAK

Promjena tlačne čvrstoće zida nakon korozije sulfatom uz visoku koncentraciju Ca^{2+}

Wei He,[a] *Xia Meng,*[b] *Yu Zheng,*[b] *Hongguang Ji*[a*] i *Chengbin Liu*[c]

U pomoćnom oknu rudnika ugljena Tong-ting u pojasu temeljne stijene pojedini dijelovi zida pokazuju različite stupnjeve propadanja. Područja na kojima je tekla voda malo su korodirana, dok su vlažni dijelovi uz izljeve izrazito korodirani. Mehanizmi te pojave najprije su proučavani kromatografijom, rendgenskom difrakcijom i energijski disperzivnom rendgenskom spektroskopijom. Veza između dubine korozije i tlačne čvrstoće te obrasca sloma analizirana je pojednostavljenim modelom utemeljenim na kôdu toka čestica (kôd toka čestica u tri dimenzije, PFC3D).

(1) Voda je prezasićena s obzirom na gips i kalcit. Dijelovi preko kojih je voda tekla zaštićeni su precipitatom na betonu. Nasuprot tome, propadanje je pojačano kristalizacijom i otapanjem u nutrini izljeva.

(2) Numerička simulacija modelom PFC3D pokazuje linearnu vezu između smanjenja vertikalnog maksimalnog naprezanja i dubine degradacije. Oštećeni dio na −355,5 m trebat će pojačati prije nego korozija dopre do 250 mm dubine.

(3) Nisu bili uočeni jasni pokazatelji propadanja prije sloma korodiranog zida. Stoga treba pratiti napredovanje propadanja prije nego uništeni dijelovi budu ojačani.

Ključne riječi
Geotehničko istraživanje, podzemna voda, propadanje, slom, naprezanje

[a] *School of Civil and Environmental Engineering,*
University of Science and Technology Beijing,
100 083 Peking, Kina
[b] *Architectural Design and Research Institute of*
Tsinghua University co., LTD, 100 084 Peking,
Kina
[c] *Beijing Vocational College of Agriculture,*
Department of Hydraulic and Architectural
Engineering, 102 442 Peking, Kina

Izvorni znanstveni rad
Prispjelo 30. rujna 2015.
Prihvaćeno 18. studenoga 2015.